crystals

MDPI

Article

A Constitutive Relation Based on the Johnson–Cook Model for Ti-22Al-23Nb-2(Mo, Zr) Alloy at Elevated Temperature

Yanju Wang [1], Duo Zhou [2], Yi Zhou [1], Aixue Sha [1], Huaxing Cheng [2] and Yabin Yan [2,*]

[1] Materials Evaluation Center for Aeronautical and Aeroengine Application, AECC Beijing Institute of Aeronautical Materials, Beijing 100095, China; yanjuwang@biam.ac.cn (Y.W.); yizhou@biam.ac.cn (Y.Z.); aixue.sha@biam.ac.cn (A.S.)

[2] Key Laboratory of Pressure Systems and Safety, Ministry of Education, School of Mechanical Power and Engineering, East China University of Science and Technology, Shanghai 200237, China; y45190047@mail.ecust.edu.cn (D.Z.); y81200043@mail.ecust.edu.cn (H.C.)

* Correspondence: yanyabin@ecust.edu.cn

Abstract: Although several schemes have been proposed to modify the classical Johnson–Cook (J-C) model, the effect of temperature on the flow stress of materials at different temperatures has not been clarified. In the current study, to investigate the deformation behavior of Ti-22Al-23Nb-2(Mo, Zr) alloy at different temperatures, uniaxial tension experiments were performed at both room (RT, 28 °C) and elevated temperatures, and a modified J-C model was developed to describe the temperature-dependent plastic flow. In tensile experiments, Ti_2AlNb-based alloy showed a continuous work hardening until reaching the ultimate strength at RT, while an apparent drop appeared in the flow stress after the peak stress at elevated temperature. Moreover, the experimental peak stress significantly depends on the testing temperature. To correctly describe the different variations of flow stresses at different temperatures, a parameter, S, which represents the softening behavior of flow stress, is integrated into the classical J-C model. In addition, the applicability and validity of the proposed J-C model were verified by calibration with experimental curves of different temperatures. On the other hand, the fractography of post-test specimens was examined to interrupt the increased fracture brittleness of Ti_2AlNb-based alloy at elevated temperatures. The proposed constitutive relation based on the J-C model is applicable to predict the deformation behavior of other Ti_2AlNb-based alloys at different temperatures.

Keywords: Ti_2AlNb alloy; mechanical properties; constitutive relation; Johnson–Cook model

Citation: Wang, Y.; Zhou, D.; Zhou, Y.; Sha, A.; Cheng, H.; Yan, Y. A Constitutive Relation Based on the Johnson–Cook Model for Ti-22Al-23Nb-2(Mo, Zr) Alloy at Elevated Temperature. *Crystals* **2021**, *11*, 754. https://doi.org/10.3390/cryst11070754

Academic Editors: Wojciech Polkowski and Pavel Lukáč

Received: 4 June 2021
Accepted: 24 June 2021
Published: 28 June 2021

1. Introduction

The ordered orthorhombic Ti_2AlNb, which was discovered in a Ti_3Al-xNb alloy in the late 1980s by Banerjee et al. [1], has attracted considerable attention as potential high-temperature structural materials for aero-engines owing to its superior performances [2–4], such as low density, high Young's modulus, specific strength, good high-temperature fatigue performance, and creep resistance. Because the actual application in aero-engines, Ti_2AlNb alloy is expected to be subject to various mechanical loads at high temperatures from 400 °C to even 1000 °C. It is critically important to precisely predict the mechanical behaviors of Ti_2AlNb alloy, including deformation and fracture, at elevated temperature for assuring the structural integrity and stability of aero-engines.

Up to now, many efforts have been devoted to the development of material systems, including composition design [5–8] and phase equilibrium and transformation [9,10], and thermal-mechanical processing techniques [11,12]. Recently, the mechanical behaviors of Ti_2AlNb alloy, such as tension [13,14], low cycle fatigue (LCF) [15], and creep [16,17], have also been discussed, and the effect of the evolution of the microstructure [18] and modification of the alloying element [19,20] was also investigated, where Mo addition was found to improve the creep resistance of Ti_2AlNb alloy [19], and Mo and Fe additions led

to the increment of the room temperature ductility of Ti_2AlNb alloys [21]. Furthermore, the stress–strain curves of Ti_2AlNb alloys with different alloy compositions and microstructures were experimentally achieved using the uniaxial tension experiments at both room and elevated temperatures [13]. The stress–strain curve at elevated temperature is usually characterized by a linear increment to a peak followed by a significant drop in flow stress, i.e., the softening of flow stress [13,22], which indicates that the representation of stress–strain curves of Ti_2AlNb alloy strongly depends on the temperature during the mechanical experiments. Therefore, the proposal of an appropriate theoretical model, which can correctly describe the stress–strain curves of Ti_2AlNb alloys at different temperatures, is a critical issue for further application in aero-engines. However, to the best knowledge of the authors, a rare investigation has been performed to develop the theoretical model to predict the deformation of Ti_2AlNb alloys at different temperatures.

In 1983, Johnson and Cook [23] proposed a general empirical constitutive model for materials subjected to a high temperature and loading rate. Until now, the J-C model has been widely applied to evaluate various metallic materials with quasi-static and high-speed impact loads at various temperatures [24–26]. However, it should be noted that the work hardening, strain rate hardening, and thermal softening are separately considered in J-C models, i.e., an uncoupled model [27–30]. In fact, during the deformation of metals at elevated temperature, the work hardening or/and strain rate hardening and thermal softening exist simultaneously and affect each other. Although the classical J-C model is applicable to the special case where the flow stress possesses a linear relation with the temperature and strain rate [23], unavoidable deviation will exist when the J-C model describes the deformation behavior under a relatively high temperature or strain rate, causing a significant nonlinear relationship with the flow stress.

In the past decade, different types of constitutive relations based on damage mechanics have been proposed to investigate the deformation behaviors of metals at elevated temperatures. Considering the effect of dislocation density, grain size, phase volume fraction, and the evolution of damage and plastic evolution, Liu et al. [31] proposed a uniform viscous plastic constitutive equation to analyze the plastic flow of Ti_2AlNb alloys at elevated temperatures of 910–970 °C. In addition, the evolution behaviors of the dislocation density, recrystallization, and grain size during thermoplastic deformation were clarified using the uniform viscous plastic relation [32]. In addition, the nucleation and growth of the intergranular cavity induced by the increment of dislocation density and grain size were discussed based on the superplasticity theory considering the evolution mechanism of damage [33]. On the other hand, besides the aforementioned constitutive relations regarding the deformation mechanisms at elevated temperatures, several modification schemes have been proposed for the classical J-C model to analyze the deformation of metals under a high temperature and strain rate [24–26,34–37]. Lin et al. [34] proposed a modified J-C model, where there was a coupling effect between yield stress and the working hardening. In addition, the influence of temperature and strain rate on the flow stress was also considered. Huh et al. [35] modified the strain rate term into a quadratic polynomial form to represent the nonlinear relation between the flow stress and the strain rate. Ulacia et al. [36] further modified the one proposed by Hub et al. [35] and defined the strain hardening exponent as a function of the strain rate, which was adopted to investigate the sensitivity of work hardening to the strain rate of magnesium alloys. By studying the stress–strain curves of magnesium alloys with different strain rates, Tan et al. [37] found that the strain rate hardening coefficient in the classical J-C model was a function of both the plastic strain and strain rate. Compared with the strain rate, the influence of temperature on the work hardening of flow stress during deformation has not been clarified. In addition, the sensitivity of the strain rate varies with the external temperature, which is induced by the change of the deformation mechanism at different temperatures. Therefore, considering the effect of temperature on the work hardening of flow stress in the J-C model is another key issue for its application in describing the deformation behaviors of materials at elevated temperatures.

In the current study, the deformation behaviors of Ti-22Al-23Nb-2(Mo, Zr) alloys (abbreviated as "Ti_2AlNb-based alloys") were experimentally investigated using uniaxial tension at both room and elevated temperatures, and corresponding stress–strain curves were obtained as well. In addition, by calibrating with the experiments, a modified J-C model considering the significant effect on the flow stress at different temperatures is developed, and its validity was examined by predicting the deformation of other specimens. Finally, the fractography of post-test specimens was carefully observed using a high-resolution field emission scanning electron microscopy (FE-SEM), and the increment of the brittle nature of fracture for Ti_2AlNb-based alloys with an increasing temperature was interrupted from the characteristic of microstructures of the fracture trace.

2. Experiments

The as-received material was a hot-rolled alloy plate with a nominal composition of Ti-22Al-23Nb-2(Mo, Zr) (at.%), and the final rolling temperature was 1020~1075 °C. After hot-rolling, the alloy was subjected to air cooling with 900~980 °C and a subsequent 2 h of annealing at 650~830 °C, respectively. Figure 1 shows the microstructure of the current Ti_2AlNb-based alloy in the SEM-BSE mode. The fine needle-like O phases are uniformly distributed on the B2 matrix in an interwoven network, where the O phase possesses a typical length of 2~5 μm and a width less than 300 nm.

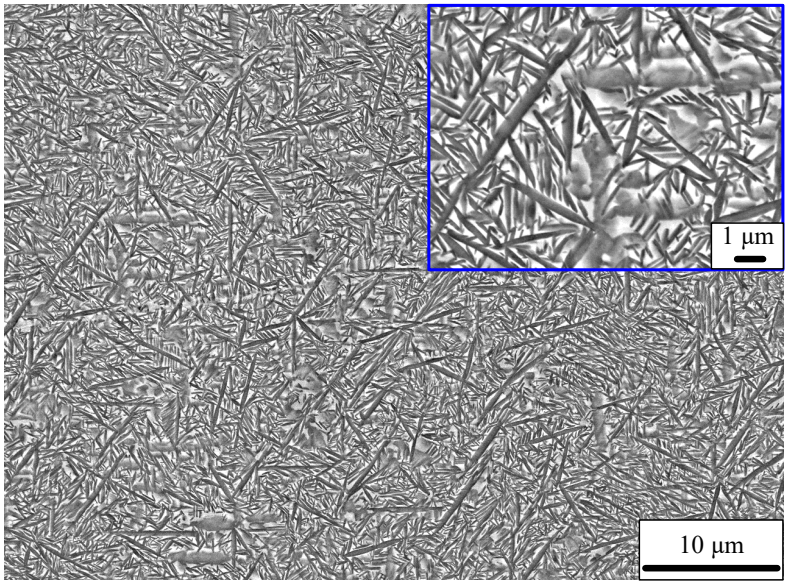

Figure 1. SEM micrograph of present Ti_2AlNb-based alloy.

Figure 2 shows the geometric dimensions of the tension specimen. The deformation behavior of the alloy was investigated by uniaxial tensile tests performed on a tension machine (Instron 5985) with a high-temperature furnace at room temperature (RT, 28 °C), 500, 550 and 650 °C, respectively. The uniaxial tension experiments were performed with a manner of displacement-control according to China National Standard of GB/T228-2010 and GB/T 228.2-2015, and the loading rate was set to 0.006 mm/mm/min for all specimens. In addition, the strain gauge was removed when the strain exceeded 5% and the loading rate was subsequently adjusted to 0.02 mm/mm/min. On the other hand, the fracture morphology of all tested specimens at different temperatures was carefully examined using a high-resolution SEM (Zeiss, Crossbeam FIB-SEM, Jena, Germany).

Figure 3 shows the true stress–strain curves of all tested specimens at RT and elevated temperature. It can be found that the deformation behavior of Ti_2AlNb-based alloy obviously changes with the increment of the temperature. At RT, the flow stress continuously increases with the applied strain until the ultimate tension strain is larger than 4%, which indicates an apparent working hardening at RT. The work hardening is also clearly identi-

fied in the flow stress of tension specimens at 500 °C, although the ultimate fracture strain is reduced to around 2%. On the other hand, with a higher temperature of 550 °C, the flow gradually increases to a peak and subsequently drops down, indicating the appearance of softening due to the high temperature. In addition, the ultimate fracture strain is further reduced to 1.5%, which is significantly smaller than the ones at RT and 500 °C. For the flow stress of the tension experiment at 650 °C, it quickly reaches a peak followed by a sharp and linear drop, showing abnormal softening. Furthermore, the ultimate fracture strain is almost the same as the one at 500 °C. Therefore, the temperature possesses a dominant effect on the deformation behavior, i.e., the flow stress, of Ti_2AlNb-based alloys, and the softening replaces the work hardening in the flow stress when the temperature is higher than 500 °C for the present study. This means that a critical transition temperature exists for the deformation of Ti_2AlNb-based alloys, and the microscopic mechanism for the deformation behavior across such a critical temperature is expected to be different as well.

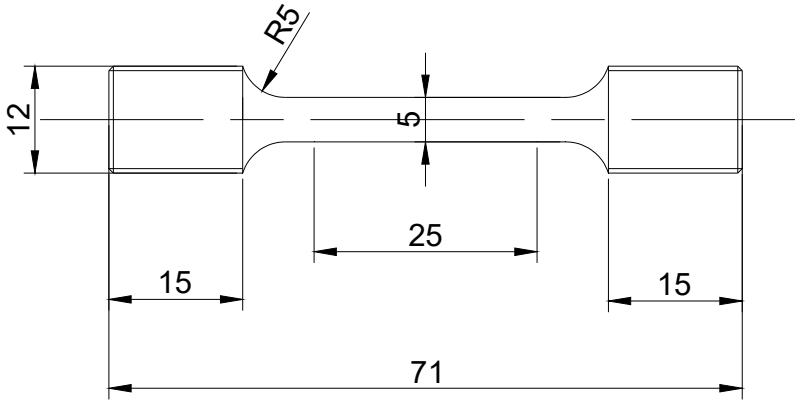

Figure 2. Geometric dimensions of the tension specimen (unit in mm).

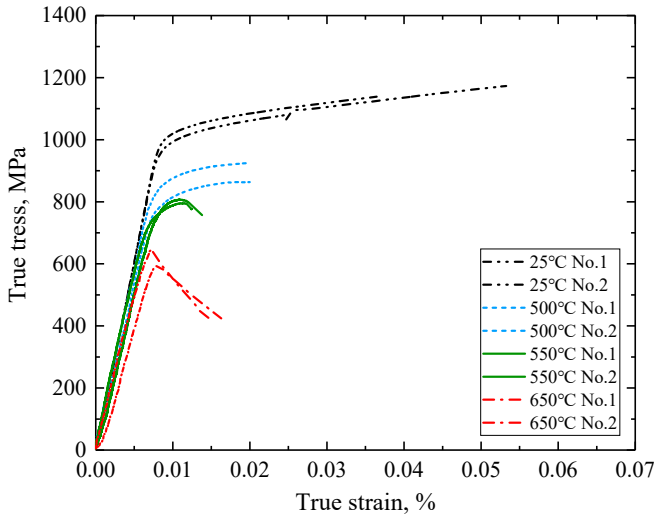

Figure 3. The true stress–strain curves of all specimens at different temperatures.

To further clarify the deformation properties of Ti_2AlNb-based alloys at different temperatures, the variation of Young's modulus and yield stress with the temperature is discussed and shown in Figure 4. As shown in Figure 4a, Young's modulus, which is determined from the slope of the experimental stress–strain curves, gradually decreases with the increment of the temperature. It is worth noting that a significant drop of Young's modulus emerges after 550 °C, which indicates the softening of Ti_2AlNb-based alloys at such elevated temperatures. On the other hand, Figure 4b illustrates the variation trend of the yield stress with the temperature. As no obvious yield point can be precisely identified from the experimental curve, the yield point is taken as the stress at which 0.2% plastic

deformation occurs, named $\sigma_{0.2}$. The yield stress also decreases with the elevation of the temperature, and a dramatic decrement appears after 550 °C as well. The similar temperature dependence of both Young's modulus and yield stress is found to be induced by the partial disordering of the O phase at the elevated temperature [38–40]. In addition, the significant drop in Young's modulus and yield stress after 550 °C indicates an intrinsic change of the deformation mechanism from the RT to the relatively high temperature.

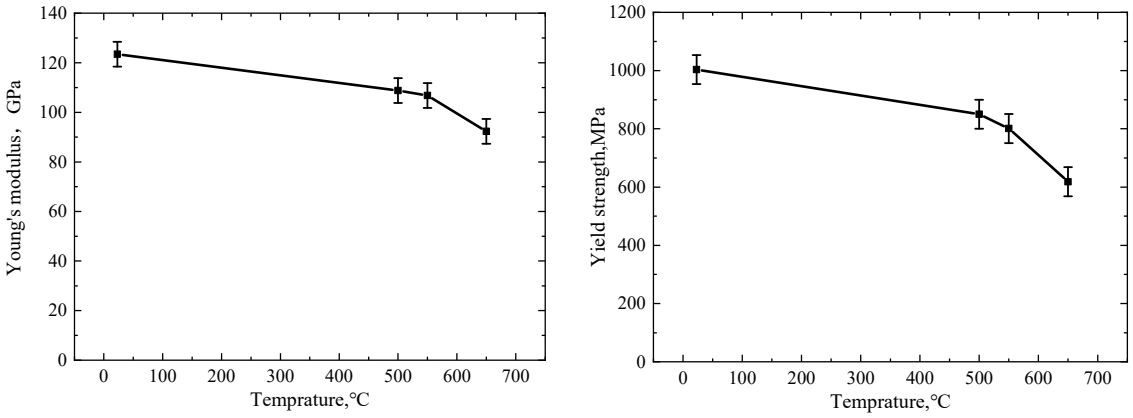

(**a**) (**b**)

Figure 4. Variation of (**a**) Young's modulus and (**b**) yield stress of Ti_2AlNb-based alloys with the temperature.

3. Constitutive Relation Based on Modified J-C Model

3.1. Classical Johnson–Cook Model

Because the tension experiments of all specimens were performed with the same loading rate, the effect of the strain rate for the J-C model is ignored in the present study. By setting the experimental strain rate to be the reference one, the classical J-C model can be simplified as:

$$\sigma = \left(A + B\varepsilon_p^n\right)\left(1 - T^{*m}\right) \tag{1}$$

Here, σ is the stress, ε_p is the plastic strain. In addition, $T^* = \frac{T - T_r}{T_m - T_r}$, where T is the experimental temperature, T_r is the room temperature, T_m is the melting temperature of materials, and A, B, m, and n are the parameters that need to be determined.

The undetermined parameters can be obtained as follows. The experimental condition of $T = T_r$ Equation (1) can be rewritten as:

$$\sigma = \left(A + B\varepsilon_p^n\right) \tag{2}$$

When the plastic strain $\varepsilon_p = 0$, $A = \sigma_{0.2}$, Equation (2) can be expressed as:

$$Ln(\sigma - A) = LnB + nLn\varepsilon_p \tag{3}$$

For the current study, based on the experimental stress–strain curve at RT, the parameters of B and n can be determined from the linear fitting of $Ln(\sigma - A)$ and $Ln\varepsilon_p$. On the other hand, for $\varepsilon_p = 0$, Equation (2) can be written as:

$$\sigma_{0.2} = A(1 - T^{*m}) \tag{4}$$

According to the yield strength in the experimental stress–strain curve at 550 °C, the temperature-sensitive parameter m can be obtained.

Figure 5 shows the comparison between the predicted stress–strain curves using the classical J-C model and experimental ones. The J-C model gives a correct prediction of the deformation behaviors of Ti_2AlNb-based alloys at both RT and 500 °C. However,

for the deformation behaviors at 550 and 650 °C, where an obvious linear drop exists in the flow stress, a significant deviation appears between the theoretical and experimental curves, indicating the inapplicability of the classical J-C model for the deformation of Ti_2AlNb-based alloys at relatively high temperatures.

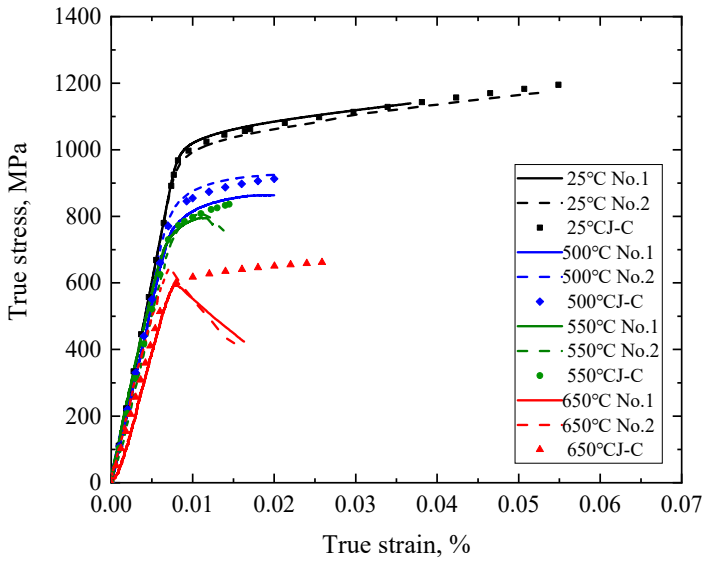

Figure 5. Comparison between the experimental and predicted stress–strain curves using the classical J-C model.

Figure 6 shows the relative difference between the experimental and theoretical flow stresses obtained from the classical J-C model. For specimens tested at the same temperature, the difference almost linearly increases with the increment of the plastic strain. On the other hand, with the increment of the temperature, the enlargement of the relative difference becomes much quicker, i.e., the slope of the relative difference–plastic strain curve becomes larger. Therefore, the relative difference shows a linear relationship with the plastic strain, and the slope of the linear relationship significantly increases with the increment of the temperature.

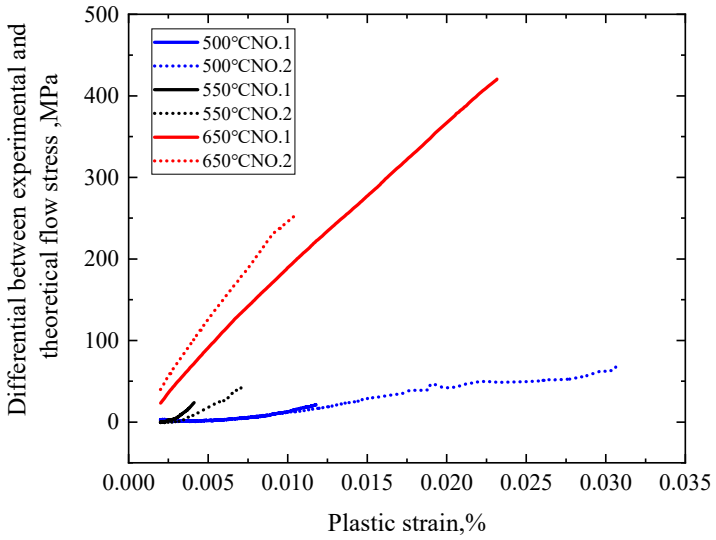

Figure 6. Variation of the difference between experimental and theoretical flow stresses at different temperatures.

3.2. Modified Johnson–Cook Model

In the classic J-C model, by regarding the yield strength at RT and the referencing strain rate to be a benchmark, the variation of stress is a function of the strain, strain rate, and temperature. Although the classic J-C model can describe the deformation behavior of materials in the temperature range from RT to the melting point, the working hardening coefficient B and n, and the strain rate hardening coefficient C are obtained from the tension tests at RT. Therefore, the deviation between the theoretical prediction from the J-C model and the experimental results enlarges with the increment of the temperature. To improve the precision of theoretical prediction, we proposed a modified J-C model considering the effect of temperature on flow stress.

Firstly, Equation (1) is written in the following form:

$$1 - \frac{\sigma}{1 - \left(A + B\varepsilon_p^n\right)\left(1 + C\dot{Ln}\dot{\varepsilon}^*\right)} = T^{*m} \tag{5}$$

where $\dot{\varepsilon}^* = \frac{\dot{\varepsilon}}{\dot{\varepsilon}_0}$. $\dot{\varepsilon}$ is the experimental strain rate and $\dot{\varepsilon}_0$ is the reference strain rate. By setting $\dot{\varepsilon}^* = 1$, the flow stress at RT is defined as $\sigma_r = \left(A + B\varepsilon_p^n\right)$. In addition, when the temperature reaches the melting point, the flow stress σ_m should be zero. Then, we have the following relation:

$$1 - \frac{\sigma}{\sigma_r} = T^{*m} \tag{6}$$

By re-writing the form of Equation (6), we have:

$$\frac{\sigma_r - \sigma}{\sigma_r - \sigma_m} = \left(\frac{T - T_r}{T_m - T_r}\right)^m \tag{7}$$

$$\sigma = \sigma_r - (\sigma_r - \sigma_m)T^{*m} \tag{8}$$

If the effect of strain rate is considered, the flow stress is obtained as:

$$\sigma = [\sigma_r - (\sigma_r - \sigma_m)T^{*m}]\left(1 + C\dot{Ln}\dot{\varepsilon}^*\right) \tag{9}$$

where $T \in [T_r, T_m]$. As aforementioned, the classical J-C model can only offer a correct prediction of the deformation behavior of Ti_2AlNb based at the temperature lower than 500 °C, which is much lower than its melting point (T_m = 1690 °C). However, a large error exists in the theoretical prediction of the J-C model for relatively high temperatures, i.e., T > 550 °C. Therefore, we define the expression of stress within a relatively high-temperature range of $T \in [T_l, T_h]$ as:

$$\sigma = [\sigma_l - (\sigma_l - \sigma_h)T^{*m}]\left(1 + C\dot{Ln}\dot{\varepsilon}^*\right) \tag{10}$$

where T_l and T_h are the lower and upper limits of the range of the elevated temperature for applying the J-C model, and σ_l, σ_h are the corresponding flow stresses with $\dot{\varepsilon}^* = 1$, which are the functions of ε_p. According to the classical J-C model, the flow stresses σ_l and σ_h can be obtained as:

$$\sigma_l = \mathrm{F}(\varepsilon_p) = \left(A_l + B_l\varepsilon_p^{n_1}\right) \tag{11}$$

$$\sigma_h = \mathrm{F}(\varepsilon_p) = \left(A_h + B_h\varepsilon_p^{n_2}\right) \tag{12}$$

To correctly predict the observed linear softening of flow stress of Ti_2AlNb-based alloys at an elevated temperature, a parameter S, representing the softening of flow stress, is introduced into the model, and Equations (11) and (12) are derived as:

$$\sigma_l = \mathrm{F}(\varepsilon_p) = \left(A_l + B_l\varepsilon_p^{n_1}\right) - S_l\varepsilon_p \tag{13}$$

$$\sigma_h = \mathrm{F}(\varepsilon_p) = \left(A_h + B_h\varepsilon_p^{n_2}\right) - S_h\varepsilon_p \quad (14)$$

Therefore, a modified J-C model considering the effect of elevated temperature on the flow stress is achieved as:

$$\sigma = \left\{\left(A_l + B_l\varepsilon_p^{n_1} - S_l\varepsilon_p\right) - \left[\left(A_l + B_l\varepsilon_p^{n_1} - S_l\varepsilon_p\right) - \left(A_h + B_h\varepsilon_p^{n_2} - S_h\varepsilon_p\right)\right]T^{*m}\right\}\left(1 + CL\dot{n}\varepsilon^*\right) \quad (15)$$

The parameters in Equations (13) and (14) can be determined using nonlinear curve fitting based on the experimental stress–strain curves at the lower and upper temperature limits. In addition, the temperature-sensitive parameter m can be derived from Equation (9) using the experiment results at the temperature limits as well. Until now, all the parameters in the modified J-C model are determined, and the flow stress at any temperature in the temperature range can be directly obtained using Equation (15). Table 1 lists all the parameters in the classical and modified J-C models.

Table 1. The definition of all parameters adopted in the current study.

Term		Term	
σ	True stress (MPa)	R	Correlation coefficient
ε_p	Plastic strain (%)	T_l	Lower limits of the range of elevated temperature
T	Experimental temperature (°C)	T_h	Upper limits of the range of elevated temperature
T_r	Room temperature (°C)	σ_l, σ_h	Corresponding flow stresses with T_l and T_h
T_m	Melting temperature (°C)	S_l, S_h	Softening constants with T_l and T_h
A	Yield stress in J-C model (MPa)	$\dot{\varepsilon}$	Experimental strain rate
B, m, n	Material constants of J-C model	$\dot{\varepsilon}_0$	Reference strain rate
$\sigma_{0.2}$	Yield stress (MPa)		

In the current study, the lower and upper temperature limits were set to 500 and 650 °C. Therefore, by using Equations (9), (13), and (14), the predicted stress–strain curves using the newly proposed modified J-C model were obtained and are shown in Figure 7. The proposed J-C model precisely predicts the total stress–strain curves, including the variation of flow stress of Ti_2AlNb-based alloys at both lower (500 °C) and upper (650 °C) temperature limits, which indicates the validity of the proposed J-C model. On the other hand, the critical transition temperature for the deformation behavior is included in the specific temperature range of 500~650 °C. However, as the detailed value of the transition temperature was not determined in the current study, the prediction of the deformation behavior at the transition temperature remains for further study.

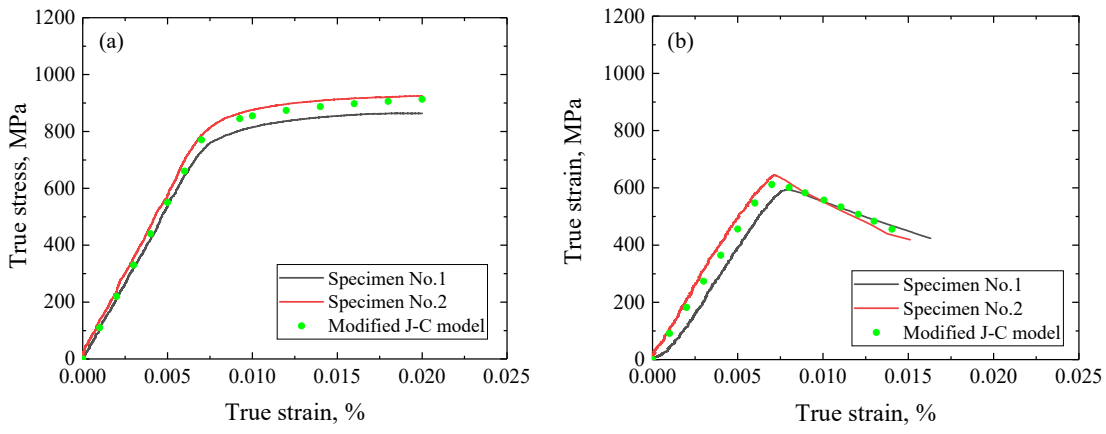

(**a**) (**b**)

Figure 7. Comparison between the experimental and the predicted stress–strain curves using the modified J-C model at (**a**) 500 °C and (**b**) 650 °C.

3.3. Validity of the Modified J-C Model

To further verify the validity and applicability of the modified J-C model, the deformation behavior of Ti_2AlNb based at 550 °C was predicted by substituting T = 550 °C into Equation (15). Figure 8 shows the comparison between the theoretically predicted and experimental stress–strain curves at 550 °C. The modified J-C model gives a very close prediction of the stress–strain curve at 550 °C as well. Therefore, it can be concluded that the modified J-C model can precisely describe the deformation behaviors of Ti_2AlNb-based alloys at any temperature within the specified range.

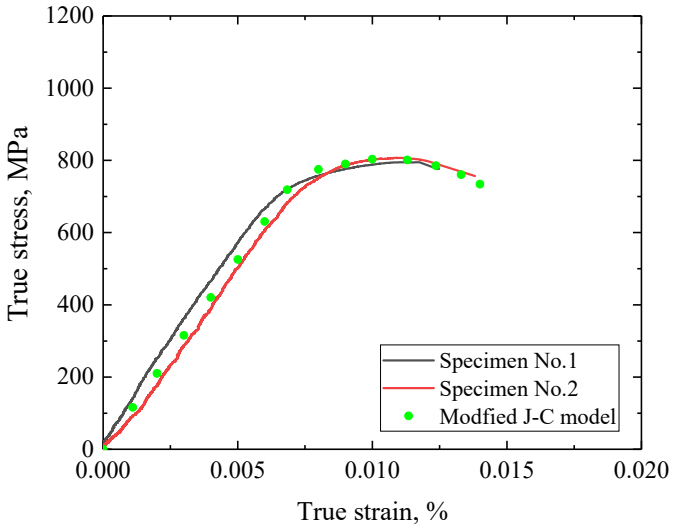

Figure 8. Predicted stress–strain curve from the modified J-C model and its comparison with the experimental result at 550 °C.

Figure 9 shows the comparison between the experimental and theoretical prediction with the classical and modified J-C models. The quality of the developed J-C model was examined using the standard statistical quantities determined by Equations (16)–(18) [41,42]. The magnitudes of R, AARE, and RMSE are 0.999, 1.3%, and 11.0 MPa determined from the modified J-C model, while 0.870, 14.5%, and 113.7 MPa were obtained from the classical model, respectively. Therefore, the proposed modified J-C model possesses an excellent precision on the prediction of deformation of Ti_2AlNb-based alloys at different temperatures.

$$\text{correlation coeffecient}\,(R) = \frac{\sum_{i=1}^{N}(E_i - E')(P_i - P')}{\sqrt{\sum_{i=1}^{N}(E_i - E')^2 \sum_{i=1}^{N}(P_i - P')^2}} \tag{16}$$

$$\text{average absolute relative error}\,(AARE) = \frac{1}{N}\sum_{i=1}^{N}\left|\frac{E_i - P_i}{E_i}\right| \tag{17}$$

$$\text{root mean square error}\,(RMSE) = \sqrt{\frac{1}{N}\sum_{i=1}^{N}(E_i - P_i)^2} \tag{18}$$

On the other hand, to further examine the robustness of the modified J-C model, the deformation behaviors of another titanium alloy of VT14 at different elevated temperatures [42] were predicted using the proposed model, and the comparison between the experimental [42] and theoretical results is shown in Figure 10. After the parameters of the modified J-C model were determined using the experimental flow stresses at the upper and lower limits of temperature range of 800–875 °C, the variation of flow stress of VT14 at 850 °C was precisely predicted by the proposed model. Therefore, the modified J-C model in the current study can predict different materials at elevated temperatures.

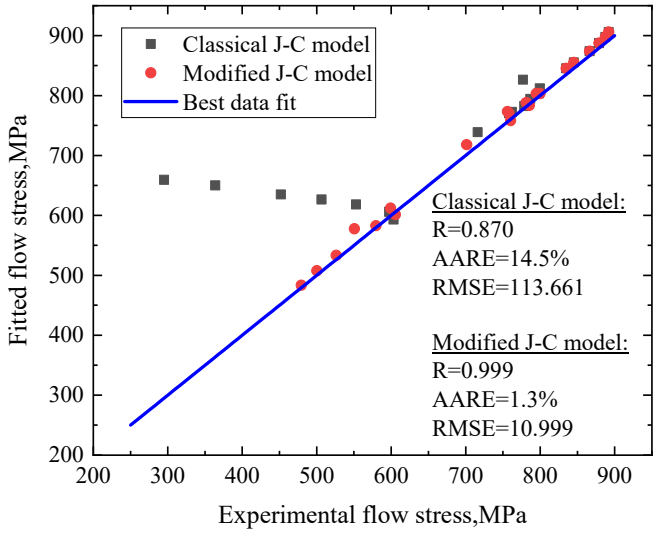

Figure 9. Correlation between experimental and fitted flow stress with the classical and modified J-C models, respectively.

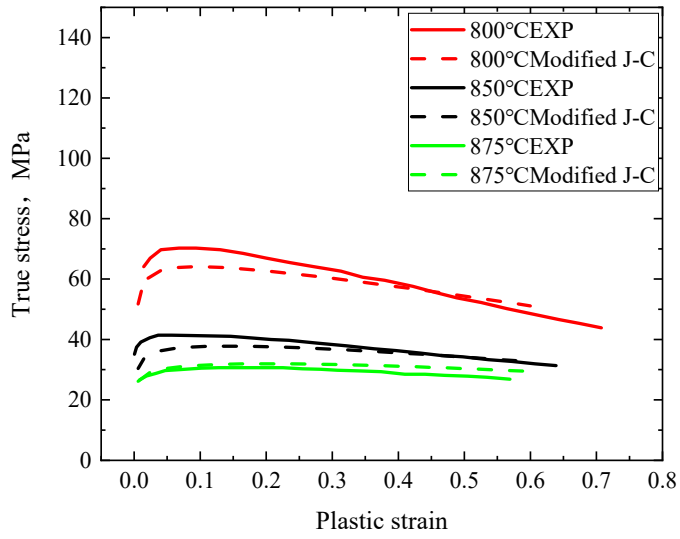

Figure 10. Comparison between experimental [42] and theoretical flow stresses of titanium alloy of VT14.

4. Temperature Dependence of Fractography with SEM Characterization

As shown in Figure 3, significant softening exists at the flow stress of Ti_2AlNb-based alloys at elevated temperatures of 550 and 650 °C in the current study. It has been well known that the dislocation motion dominates the plastic deformation of metals. With an increase of the temperature, the motion resistance due to Peierls–Nabarro stress is reduced and thus the dislocation motion becomes easier than that at RT [43–45]. On the other hand, as the yield strength is sensitive to the Peierls–Nabarro stress [44], and thus the yield strength of materials becomes lower as well. Therefore, the weakened resistance of dislocation motion induced by the elevated temperature causes softening in the flow stress of Ti_2AlNb-based alloys.

On the other hand, to further clarify the significant drop of flow stress at an elevated temperature, we examined the fractography of post-test specimens at different temperatures using FE-SEM. Figure 11 shows the overall views of fracture surfaces and the high magnification observation of corresponding microscopic characteristics of the tested specimens at RT, 550 °C, and 650 °C, respectively. For the fracture surface at RT, a typical mixture of intergranular and transgranular fractures is identified from the overall view (Figure 11a). The appearance of cleavage steps further confirms the existence of intergranular fracture

(Figure 11b). Therefore, the co-existence of intergranular and transgranular fractures results in relatively good plasticity and a large ultimate fracture strain of Ti_2AlNb-based alloys at RT. On the other hand, at the elevated temperature, an apparent drop emerges in the flow stress and the ultimate fracture strain is reduced as well. As shown in Figure 11c, the overall view of fracture surface at 550 °C indicates that the proportion of transgranular fracture is largely increased, and secondary cracks also appear. A close observation of the typical zone of the fracture surface, as shown in Figure 11d, shows that dimples appear, and the cleavage fracture still exists. This means that, although the plastic deformation indicated by dimples is strengthened, the transgranular fracture and appearance of secondary cracks cause the brittle nature of Ti_2AlNb-based alloys at 550 °C. Finally, the fracture surface at 650 °C in Figure 11e,f clearly illustrates the predominance of transgranular fracture and the increased number of secondary cracks, which causes the significant softening of flow stress at 650 °C. Therefore, the SEM characterization of the fractography indicates the transition of the deformation behavior of Ti_2AlNb-based alloy at different temperatures is mainly represented by the variation of the fracture mechanism from the mixture of intergranular and transgranular fractures to the dominance of the trangranular fracture and secondary crack. In addition, the linearity of the relative difference between the experimental and theoretical results with the temperature suggests that the proposed parameter can be adopted to approximately evaluate the transition of the fracture mechanism during the increment of the testing temperature.

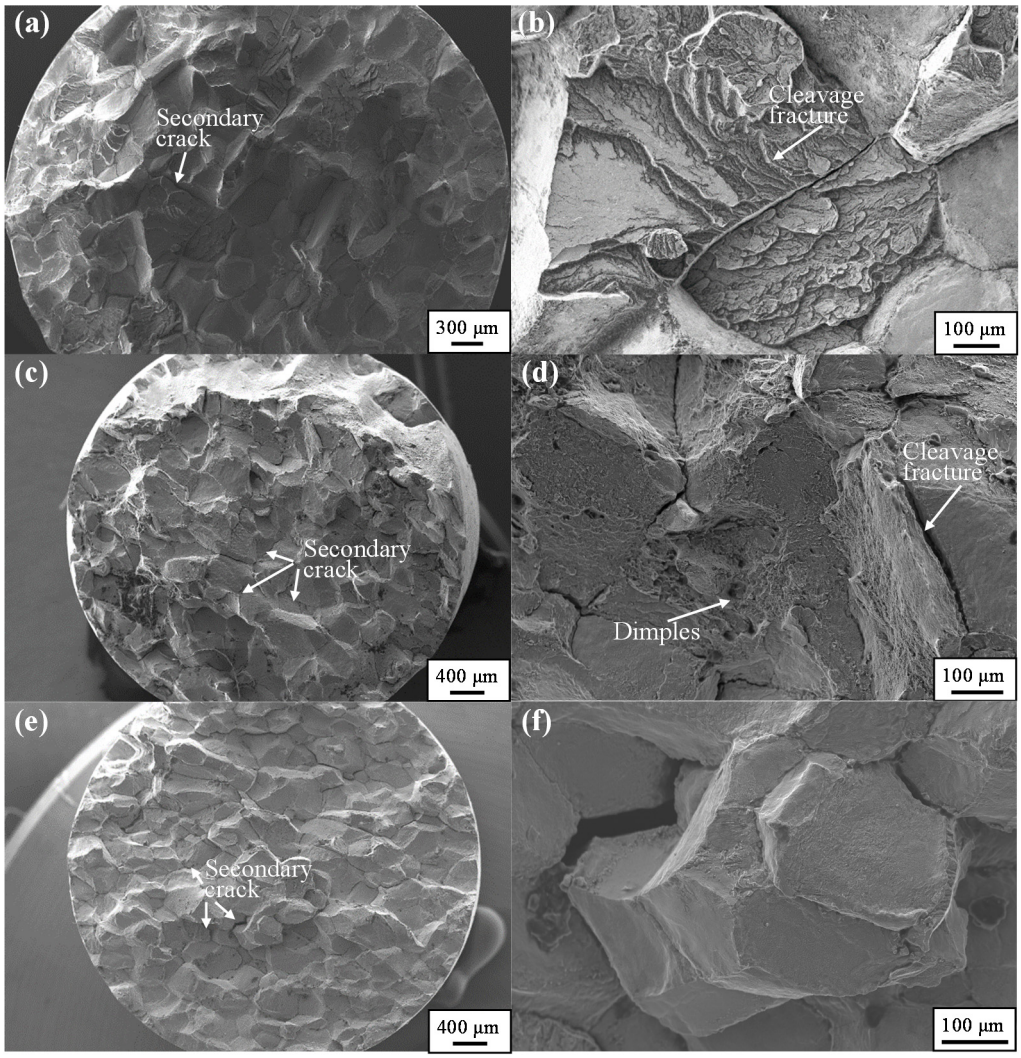

Figure 11. Fracture surfaces of post-test specimens at (**a**,**b**) RT, (**c**,**d**) 550 °C, and (**e**,**f**) 650 °C.

On the other hand, it was found that Ti_2AlNb-based alloys generally show high hardness and significant brittleness due to the characteristic complex of long-range-ordered crystal structures [46]. In addition, cleavage or intergranular fracture dominates the failure of Ti_2AlNb-based alloys at low homologous temperatures, i.e., the brittle-to-ductile transition temperature (DBTT). In the current study, although the tension experiments in the current study were performed at elevated temperatures of up to 650 °C, the testing temperature in the current study was still lower than the DBTT of Ti_2AlNb-based alloys [46]. Therefore, although the elevated temperature improved the motion of dislocation and induced the decrement of yield stress, the fracture of all tested specimens were brittle ones. In addition, the analysis of the fractography of all tested specimens further confirms the brittleness of fracture of all specimens in the current study.

5. Conclusions

The deformation behavior of Ti_2AlNb-based alloys was investigated using uniaxial tension experiments at RT and elevated temperature, and a modified J-C model was proposed to describe the observed variation of flow stress at different temperatures. The main results are summarized as follows.

1. Uniaxial tension experiments at different temperatures revealed the dominant effect of temperature on the deformation of Ti_2AlNb-based alloys. Both Young's modulus and yield strength decreased with the increment of the temperature. Furthermore, different from RT, obvious softening of the flow stress was observed in experiments at 550 and 650 °C;
2. The classical J-C model was found to fail to describe the softening of flow stress at the relatively high temperature, although it gave a correct prediction of the deformation of Ti_2AlNb-based alloys at RT;
3. A modified J-C model was developed by introducing an extra parameter to represent the linear drop of flow stress at elevated temperatures. After determining the corresponding parameters of the J-C model with the experimental results of the lower and upper temperature limits, the deformation behavior at any temperature belonging to the specific range can be correctly described.
4. The fractography of post-test specimens at different temperatures was characterized by FE-SEM. Besides the decrement of resistance to dislocation motion due to the elevated temperature, the softening of flow stress was strongly dependent on the increased proportion of transgranular fracture and the existence of a secondary crack in Ti_2AlNb-based alloys.

This work provides important insight into the deformation and fracture behaviors of Ti_2AlNb alloys at both RT and elevated temperature, and a powerful and precise theoretical model to predict its deformation at any temperature within a required range, which is the critical issue for the application Ti_2AlNb alloys at elevated temperatures.

Author Contributions: Writing—original draft preparation Conceptualization, Y.W.; methodology, resources, Y.Z. and A.S.; formal analysis, visualization, D.Z. and H.C.; Conceptualization, validation, writing—review and editing, supervision, Y.Y.; All authors have read and agreed to the published version of the manuscript.

Funding: This research was funded by Natural Science Foundation of Shanghai (Grant No. 19ZR1413200), Program for Professor of Special Appointment (Eastern Scholar) at Shanghai Institutions of Higher Learning, Major Project for Aero Engine-Gas Turbine of Ministry of Industry and Information Technology, China (KH1B191503), Stably supporting key project of State Administration of Science, Technology and Industry for National Defense, China (KZ0C191708).

Informed Consent Statement: Not applicable.

Data Availability Statement: The raw/processed data required to reproduce these findings cannot be shared at this time as the data also forms part of an ongoing study.

Acknowledgments: This work was supported by Natural Science Foundation of Shanghai (Grant No. 19ZR1413200), Program for Professor of Special Appointment (Eastern Scholar) at Shanghai Institutions of Higher Learning, Major Project for Aero Engine-Gas Turbine of Ministry of Industry and Information Technology, China (KH1B191503), Stably supporting key project of State Administration of Science, Technology and Industry for National Defence, China (KZ0C191708).

Conflicts of Interest: The authors declare no conflict of interest. The funders had no role in the design of the study; in the collection, analyses, or interpretation of data; in the writing of the manuscript, or in the decision to publish the results.

References

1. Banerjee, D.; Gogia, A.K.; Nandi, T.K. A new ordered orthorhombic phase in a Ti_3AlNb alloy. *Acta Metall.* **1988**, *36*, 871–882. [CrossRef]
2. Wu, X. Review of alloy and process development of TiAl alloys. *Intermetallics* **2006**, *14*, 1114–1122. [CrossRef]
3. Bo, W.; Zinkevich, M.; Aldinger, F.; Chu, M.; Shen, J. Prediction of the ordering behaviours of the orthorhombic phase based on Ti_2AlNb alloys by combining thermodynamic model with ab initio calculation. *Intermetallics* **2008**, *16*, 42–51.
4. Dey, S.R.; Roy, S.; Suwas, S. Annealing response of the intermetallic alloy Ti-22Al-25Nb. *Intermetallics* **2010**, *18*, 1122–1131. [CrossRef]
5. Mao, Y.; Hagiwara, M.; Emura, S. Creep behavior and tensile properties of Mo- and Fe-added orthorhombic Ti-22Al-11Nb-2Mo-1Fe alloy. *Scr. Mater.* **2007**, *57*, 261–264. [CrossRef]
6. Chen, X.; Weidong, Z.; Wei, W.; Xiaobo, L.; Jianwei, Z. The enhanced tensile property by introducing bimodal size distribution of lamellar O for O+B2 Ti_2AlNb based alloy. *Mater. Sci. Eng. A* **2013**, *587*, 54–60. [CrossRef]
7. Germann, L.; Banerjee, D.; Guedou, J.Y. Effect of composition on the mechanical properties of newly developed Ti_2AlNb-based titanium aluminide. *Intermetallics* **2005**, *13*, 920–924. [CrossRef]
8. Wen, Y.F.; Wang, L.; Liu, H.L.; Song, L. Ab initio study of the elastic and mechanical properties of B19 TiAl. *Crystals* **2017**, *7*, 39. [CrossRef]
9. Shao, B.; Zong, Y.; Wen, D.; Tian, Y.; Shan, D. Investigation of the phase transformations in Ti-22Al-25Nb alloy. *Mater. Charact.* **2016**, *114*, 75–78. [CrossRef]
10. Shao, B.; Wan, S.; Xu, W.; Shan, D.; Guo, B.; Zong, Y. Formation mechanism of an α2 phase-rich layer on the surface of Ti-22Al-25Nb alloy. *Mater. Charact.* **2018**, *145*, 205–209. [CrossRef]
11. Wu, Y.; Wang, D.; Liu, Z.; Liu, G. A unified internal state variable material model for Ti_2AlNb-alloy and its applications in hot gas forming. *Int. J. Mech. Sci.* **2019**, *164*, 105126. [CrossRef]
12. Xue, C.; Zeng, W.; Wang, W. Quantitative analysis on microstructure evolution and tensile property for the isothermally forged Ti_2AlNb based alloy during heat treatment. *Mater. Sci. Eng. A* **2013**, *573*, 183–189. [CrossRef]
13. Lin, P.; He, Z.; Yuan, S. Tensile deformation behavior of Ti-22Al-25Nb alloy at elevated temperatures. *Mater. Sci. Eng. A* **2012**, *556*, 617–624. [CrossRef]
14. Cai, J.; Wang, K.; Zhai, P. A Modified Johnson-Cook Constitutive Equation to Predict Hot Deformation Behavior of Ti-6Al-4V Alloy. *J. Mater. Eng. Perform.* **2015**, *24*, 32–44. [CrossRef]
15. Yinling, Z.; Aihan, F.; Shoujiang, Q. Microstructure and low cycle fatigue of a Ti_2AlNb-based lightweight alloy. *J. Mater. Sci. Technol.* **2020**, *44*, 140–147.
16. Nandy, T.K.; Banerjee, D. Creep of the orthorhombic phase based on the intermetallic Ti_2AlNb. *Intermetallics* **2000**, *8*, 915–928. [CrossRef]
17. Jiao, X.; Liu, G.; Wang, D. Creep behavior and effects of heat treatment on creep resistance of Ti-22Al-24Nb-0.5Mo alloy. *Mater. Sci. Eng. A* **2017**, *680*, 182–189. [CrossRef]
18. Zhang, N.; Han, X.; Sun, D. Microstructure evolution and mechanical properties of LaB_6-modified Ti_2AlNb alloy fabricated by blended elemental powder metallurgy. *Powder Technol.* **2020**, *369*, 334–344. [CrossRef]
19. Wei, W.; Zeng, W.; Dong, L.; Zhu, B.; Zheng, Y.; Liang, X. Microstructural evolution and tensile behavior of Ti_2AlNb alloys based α2-phase decomposition. *Mater. Sci. Eng. A* **2016**, *662*, 120–128.
20. Zhang, Y.; Liu, Y.; Yu, L. Microstructures and tensile properties of Ti_2AlNb and Mo-modified Ti_2AlNb alloys fabricated by hot isostatic pressing. *Mater. Sci. Eng. A* **2020**, *776*, 139043. [CrossRef]
21. Emura, S.; Tsuzaki, K.; Tsuchiya, K. Improvement of room temperature ductility for Mo and Fe modified Ti_2AlNb alloy. *Mater. Sci. Eng. A* **2010**, *528*, 355–362. [CrossRef]
22. Wang, H.P.; Liu, D.; Wang, J.G.; Shi, Y.Z.; Zheng, Y.; Hu, Y. Investigation on the thermal deformation behavior of the nickel-based superalloy strengthened by γ' phase. *Crystals* **2019**, *9*, 125. [CrossRef]
23. Johnson, G.R.; Cook, W.H. A constitutive model and data for metals subjected to large strains high strain rates and high temperatures. In Proceedings of the Seventh International Symposium on Ballistics, The Hague, The Netherlands, 19–21 April 1983; Volume 21, pp. 541–548.
24. Zhang, D.; Shangguan, Q.; Xie, C. A modified Johnson-Cook model of dynamic tensile behaviors for 7075-T6 aluminum alloy. *J. Alloys Compd.* **2015**, *619*, 186–194. [CrossRef]

25. Li, H.Y.; Wang, X.F.; Duan, J.Y. A modified Johnson Cook model for elevated temperature flow behavior of T24 steel. *Mater. Sci. Eng. A* **2013**, *577*, 138–146. [CrossRef]
26. Mirkoohi, E.; Tran, H.C.; Lo, Y.L.; Chang, Y.C.; Lin, H.Y.; Liang, S.Y. Analytical modeling of residual stress in laser powder bed fusion considering part's boundary condition. *Crystals* **2020**, *10*, 337. [CrossRef]
27. Shrot, A.; Bäker, M. Determination of Johnson–Cook parameters from machining simulations. *Comput. Mater. Sci.* **2012**, *52*, 298–304. [CrossRef]
28. Lin, Y.C.; Liu, G. A new mathematical model for predicting flow stress of typical high-strength alloy steel at elevated high temperature. *Comput. Mater. Sci.* **2010**, *48*, 54–58. [CrossRef]
29. Samantaray, D.; Mandal, S.; Bhaduri, A.K. A comparative study on Johnson-Cook, modified Zerilli-Armstrong and Arrhenius type constitutive model to predict elevated temperature flow behaviour in modified 9Cr-1Mo steel. *Comput. Mater. Sci.* **2019**, *47*, 568–576. [CrossRef]
30. Samantaray, D.; Mandal, S.; Borah, U. A thermo-viscoplastic constitutive model to predict elevated-temperature flow behaviour in a titanium-modified austenitic stainless steel. *Mater. Sci. Eng. A* **2009**, *526*, 1–6. [CrossRef]
31. Liu, Z.; Wang, X.; Jiao, X.; Wu, Y.; Liu, G. Prediction of microstructure evolution during hot gas forming of Ti_2AlNb-based alloy tubular component with square cross-section. *Procedia Manuf.* **2018**, *15*, 1156–1163. [CrossRef]
32. Lin, J.; Liu, Y. A set of unified constitutive equations for modelling microstructure evolution in hot deformation. *J. Mater. Process. Technol.* **2003**, *143*, 281–285. [CrossRef]
33. Lin, J.; Cheong, B.H.; Yao, X. Universal multi-objective function for optimising superplastic-damage constitutive equations. *J. Mater. Process. Technol.* **2002**, *125*, 199–205. [CrossRef]
34. Lin, Y.C.; Chen, X.M.; Liu, G. A modified Johnson-Cook model for tensile behaviors of typical high-strength alloy steel. *Mater. Sci. Eng. A* **2010**, *527*, 6980–6986. [CrossRef]
35. Huh, H.; Kang, W.J.; Han, S.S. A tension split Hopkinson bar for investigating the dynamic behavior of sheet metals. *Exp. Mech.* **2002**, *42*, 8–17. [CrossRef]
36. Ulacia, I.; Salisbury, C.P.; Hurtado, I. Tensile characterization and constitutive modeling of AZ31B magnesium alloy sheet over wide range of strain rates and temperatures. *J. Mater. Process. Tech.* **2011**, *211*, 830–839. [CrossRef]
37. Tan, J.Q.; Zhan, M.; Liu, S. A modified Johnson-Cook model for tensile flow behaviors of 7050-T7451 aluminum alloy at high strain rates. *Mater. Sci. Eng. A* **2015**, *631*, 214–219. [CrossRef]
38. Chu, F.; Mitchell, T.E.; Majumdar, B.; Miracle, D.; Nandy, T.K.; Banerjee, D. Elastic properties of the O phase in Ti-Al-Nb alloys. *Intermetallics* **1997**, *5*, 147–156. [CrossRef]
39. Banerjee, D. The intermetallic Ti_2AlNb. *Prog. Mater. Sci.* **1997**, *42*, 135–158. [CrossRef]
40. Kumpfert, J. Intermetallic alloys based on orthorhombic titanium aluminide. *Adv. Eng. Mater.* **2001**, *3*, 851–864. [CrossRef]
41. Mosleh, A.O.; Mikhaylovskaya, A.V.; Kotov, A.D.; Kwame, J.S. Experimental, modelling and simulation of an approach for optimizing the superplastic forming of Ti-6%Al-4%V titanium alloy. *J. Manuf. Process.* **2019**, *45*, 262–272. [CrossRef]
42. Mosleh, A.O.; Mestre-Rinn, P.; Khalil, A.M.; Kotov, A.D.; Mikhaylovskaya, A.V. Modelling approach for predicting the superplastic deformation behaviour of titanium alloys with strain hardening/softening characterizations. *Mater. Res. Express* **2020**, *7*, 016504. [CrossRef]
43. Wu, Z.; Hu, R.; Zhang, T. Microstructure determined fracture behavior of a high Nb containing TiAl alloy. *Mater. Sci. Eng. A* **2016**, *666*, 297–304. [CrossRef]
44. Hertzberg, R.W.; Hauser, F.E. Deformation and Fracture Mechanics of Engineering Materials. *J. Mater. Sci. Technol.* **1997**, *19*, 283–286. [CrossRef]
45. Zhou, M.; Clode, M.P. Constitutive equations for modelling flow softening due to dynamic recovery and heat generation during plastic deformation. *Mech. Mater.* **1998**, *27*, 63–76. [CrossRef]
46. Ritchie, R.O. Mechanisms of fatigue-crack propagation in ductile and brittle solids. *Int. J. Fract.* **1999**, *100*, 55–83. [CrossRef]